Evidence of double-gap superconductivity in noncentrosymmetric $Nb_{0.18}Re_{0.82}$ single crystals

C. Cirillo,[1] R. Fittipaldi,[1] M. Smidman,[2] G. Carapella,[1] C. Attanasio,[1] A. Vecchione,[1] R. P. Singh,[2] M. R. Lees,[2] G. Balakrishnan,[2] and M. Cuoco[1]

[1]*CNR-SPIN and Dipartimento di Fisica "E. R. Caianiello", Università di Salerno, I-84084 Fisciano (Salerno), Italy*

[2]*Department of Physics, University of Warwick, Coventry CV4 7AL, United Kingdom*

(Received 14 November 2014; revised manuscript received 3 April 2015; published 20 April 2015)

We combine point contact spectroscopy with specific heat measurements to probe the superconducting state in noncentrosymmetric $Nb_{0.18}Re_{0.82}$ single crystals. The conductance spectra clearly exhibit a two-peak structure that is well reproduced within a two-band model with isotropic gaps in the spectrum. Such an observation is confirmed by distinct features of the specific heat both at low temperatures and in the range approaching the transition to the normal state. The analyses provide convincing evidence that the two-gap superconducting pairing is a robust feature of $Nb_{0.18}Re_{0.82}$.

DOI: 10.1103/PhysRevB.91.134508 PACS number(s): 74.70.Ad, 74.45.+c, 74.25.Bt, 74.20.Rp

I. INTRODUCTION

Time reversal and inversion are two fundamental symmetries that set the character of the superconducting pairing. If both are present the superconducting order parameter can be grouped into even and odd parity corresponding to spin-singlet and spin-triplet configurations, respectively [1]. The absence of time reversal symmetry generally leads to a suppression of the spin-singlet pairing which can be easily achieved by applying an external magnetic field. A different scenario occurs for inversion symmetry breaking as due to large screening of the electric field in a metal, it is difficult to induce with external sources. It is the lack of a center of inversion in the crystal structure that allows parity to be violated and the effects of this on the properties of the superconducting phase can be studied. The discovery of superconductivity in the heavy-fermion compound $CePt_3Si$ [2] has motivated intense experimental and theoretical studies [3] since its crystal symmetry lacks a center of inversion. The parity violation leads to a classification scheme of the pairing symmetry different from the standard one, indeed the admixture of spin-singlet and spin-triplet pairing states is expected to occur [4–7].

As a consequence of inversion symmetry breaking, exotic properties have been predicted and observed, such as multigap and nodal superconductivity [8–11], large upper critical fields [12–14], nontrivial quantum topology in the superconducting ground state [15], as well as charge and spin currents along the edge [16]. The understanding of the nature of the pairing and the mechanisms that lead to superconductivity in materials without inversion symmetry is thus a fundamental and highly debated issue in the field of unconventional superconductors.

In the past few years a growing number of noncentrosymmetric superconductors (NCS) have been studied, varying from heavy-fermion compounds to a number of weakly correlated intermetallic materials [3]. In heavy-fermions NCS it is suggested that nonphonon mechanisms provide the pairing glue because superconductivity occurs in the vicinity of magnetic phases. If pairing is mediated by spin fluctuations, it is plausible that they lead to interactions that favor the parity mixing of Cooper pairs involving different angular momentum channels. Even when the antisymmetric spin-orbit coupling is smaller than the relevant electronic scale of energies close to the Fermi level, it is possible that under specific conditions the parity mixing becomes relevant for the formation of the pairing states. For instance, when the attractive pairing interactions in the spin-singlet and spin-triplet channels are comparable in magnitude, the antisymmetric spin-orbit can lead to strong mixing of these two states. Due to the presence of many competing interactions, the resulting physical scenario is highly nontrivial and it is difficult to predict which channel might dominate in determining the superconducting state of noncentrosymmetric materials. Another complication that emerges when attempting to single out the role of inversion symmetry breaking in the superconducting phase is that many NCS materials exhibit a complex electronic structure, with many orbitals close to the Fermi level.

In weakly correlated transition metal compounds which do not exhibit magnetic complexity as in the heavy-fermion case, e.g., Ru_7B_3, $AMSi_3$ (A = Ca, Sr, La, and Ba and M = Co, Rh, Ir, Ni, Pd, and Pt), $Mg_{10}Ir_{19}B_{16}$, Mo_3Al_2C, and Re_3W [17–21], conventional s-wave behavior has been often reported. An exception is in the case of Re_6Zr, for which muon spin relaxation measurements reveal the presence of a spontaneous magnetic field below the critical temperature T_c providing evidence for a superconducting state with time reversal symmetry breaking [22]. In the case of Nb_xRe_{1-x}, measurements on polycrystalline samples with $x = 0.18$ confirm that it is a type-II superconductor with a bulk transition temperature $T_c \sim 8.8$ K [23,24]. The exponential activation in the low-temperature behavior of the thermodynamic responses has been interpreted in terms of a single isotropic gap. Similar behavior led to the same conclusions for the case of Nb_xRe_{1-x} with x in the range [0.13–0.38] [25]. Anomalies were pointed out in connection with the high value of the specific heat jump indicating that the compound is in the moderate-coupling regime. However, since the upper critical field is quite close to the estimated Pauli limiting field, further investigations on high-quality single crystals are required to clarify whether a possible mixture of singlet and triplet pairing states or other scenarios occur in the NCS Nb_xRe_{1-x} [23,25].

In this paper, benefiting from the successful achievement in the synthesis of high quality single crystals of noncentrosymmetric $Nb_{0.18}Re_{0.82}$ [26], we obtain more insight into the nature of the superconducting state by combining point contact spectroscopy and specific-heat measurements. We find that the conductance spectra clearly exhibit a two-peak structure at finite applied bias, whose temperature dependence can be

well described by a minimal two-band model with spin-singlet isotropic gaps. The two-gap features have been observed in different sets of measurements providing convincing evidence that the multicomponent character of the superconducting state of noncentrosymmetric $Nb_{0.18}Re_{0.82}$ is a robust feature. To exclude the possibility of a surface reconstruction of the superconducting state, a careful analysis of the temperature dependence of the specific heat demonstrates that a model with a single isotropic gap is unable to reproduce both the low- and high-temperature behavior (close to T_c), whereas this can be accounted for within a two-gap model.

The paper is organized as follows. In Sec. II we present the experimental methodology. Section III is devoted to the results of the point contact spectroscopy and the specific heat measurements as well as the related discussions. Finally, in Sec. IV we provide the concluding remarks.

II. EXPERIMENTAL DETAILS

Single crystals of Nb_xRe_{1-x} with $x = 0.18$ have been synthesized by the floating zone technique using a four mirror optical furnace with Xe arc lamps as described in detail in Ref. [26]. Crystals of large volume and high quality have been obtained whose morphology and composition were checked by a scanning electron microscope (SEM) equipped with an energy dispersive spectrometer (EDS). Moreover, the Laue back reflection technique was employed to specifically orient the single crystals with one of the principal symmetry axes (referred to as the c axis) perpendicular to their surface for the design of the point contact experimental configuration. Sharp and clear spots were obtained, which agree with the $I\bar{4}3m$ (no. 217) symmetry of the crystal [26]. A representative Laue pattern of an oriented $Nb_{0.18}Re_{0.82}$ crystal is shown in Fig. 1.

The samples used for the measurement were about $3 \times 2 \times 1$ mm^3 and were polished along the ab symmetry plane. Before performing the electrical characterization, the crystals were etched in a mixture of HF, HNO_3, and H_3PO_4 in order to remove any deteriorated surface layers. Transport properties were investigated using a standard dc four-probe technique in zero magnetic field down to $T = 300$ mK, in a sorption pumped ^{3}He HelioxVL insert from Oxford Instruments. A set of preliminary characterizations was performed to determine both the value of T_c and the residual resistivity ratio (RRR), defined as $RRR \equiv \rho(T = 300\ \mathrm{K})/\rho(T = 10\ \mathrm{K})$. The resulting values were $T_c \sim 8.5$ K and $RRR = 1.14$. Then, point contact spectroscopy was performed for the analyzed samples by means of the widely used *soft contact* technique [27–30] that consists of having a small drop of Ag conductive paint as a counterelectrode on the freshly etched surface of the crystal below a 25-μm-diameter gold wire [see Fig. 2(a)]. In this configuration the conducting regime can be tuned by applying short voltage pulses to the junction [27,31], which is different from conventional point contact, where similar control is achieved by varying the pressure between the tip and the sample. The values of the contact resistance for all the spectra reported in this work were always lower than $R_c = 10\ \Omega$. The diameter of the effective contact area a can be roughly estimated according to the Sharvin formula $R_c = 4\rho_0 l/3\pi a^2$, with the low temperature resistivity of the crystal being $\rho_0 = 120\ \mu\Omega$ cm [26]. Concerning the mean free path, in Ref. [25] a value of $l \approx 5$ nm was estimated, which would result in $a \approx 6$–40 nm. These estimates are consistent with the average dimensions of the Ag grains on the surface of the superconductor, as one can observe from Fig. 2(b) [29], and with the values of the samples roughness, which is of the order of 50 nm. Therefore, it is reasonable to conclude that the point contact junctions are close to the ballistic regime. It is worth pointing out that in the soft contact configuration, R_c is the resistance of the parallel arrangement of grains, which individually are more resistive. This conclusion is further

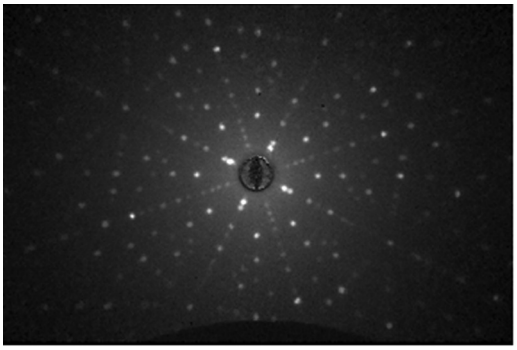

FIG. 1. X-ray Laue pattern of a $Nb_{0.18}Re_{0.82}$ crystal oriented with one of the principal axes perpendicular to the exposed surface.

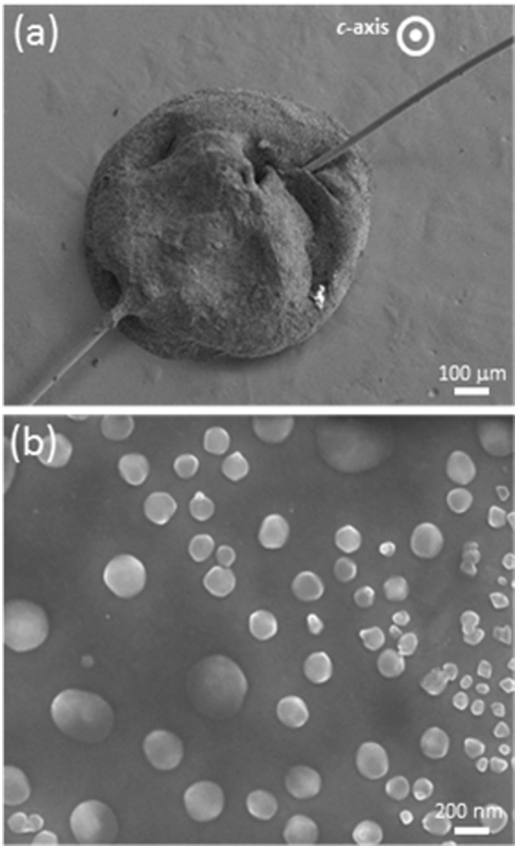

FIG. 2. Field emission scanning electron microscope image of (a) the $Nb_{0.18}Re_{0.82}$ single crystal (ab plane) with Au wire and silver paste drop and (b) the Ag particles on the measured $Nb_{0.18}Re_{0.82}$ surface after removing the gold wire.

supported by the absence of any downward curvature or sharp dips in the spectra, which could be a signature of heating or in general, of nonideal conduction through the contact [27].

I-V curves were recorded by biasing the junction with a pulsed current (current-on time was 12 ms, current-off time was 1 s) along the c axis. The conductance curves dI/dV vs V were obtained by numerical differentiation of the measured I-V characteristics. Hence, a systematic study of the temperature dependence of the conductance spectra (dI/dV vs V) was performed.

In addition, specific-heat measurements were made using the two-τ relaxation method with a Quantum Design Physical Property Measurement System. A ^{3}He insert was used for zero field measurements down to 400 mK.

III. RESULTS

In this section we present an analysis of the superconducting state obtained by means of point contact spectroscopy and specific heat measurements.

A. Point contact spectroscopy

In Fig. 3 we report representative normalized conductance spectra obtained by means of point contact spectroscopy on an oriented single crystal (sample 1). As one can note the low-temperature data show a dominant peak structure at $V_B \sim \pm 1.1$ meV and a satellite shoulder at higher energies with a maximum at about $V_A \sim \pm 2.0$ meV. There is no evidence of midgap bound states and the spectral weight in the gap is not significantly suppressed, thus revealing that a good

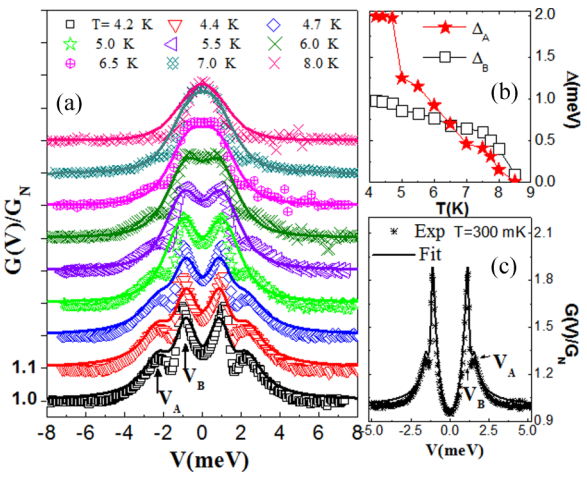

FIG. 3. (Color online) (a) Temperature dependence of the conductance spectra measured from 4.2 to 8.0 K. For clarity, the data are plotted with a constant offset along the linear vertical scale. The symbols are the experimental data and the solid lines are the fits to the data using the isotropic two-gap model as discussed in the main text. The arrows schematically indicate the positions of the dominant peaks in the spectrum at voltage biases V_A and V_B. (b) Temperature dependence of the gaps Δ_A and Δ_B as extracted from the fits to the conductance spectra. (c) Conductance spectrum measured at $T = 300$ mK at another position of the $Nb_{0.18}Re_{0.82}$ surface with respect to that in (a). This spectrum also exhibits the double gap structures at voltage biases V_A and V_B.

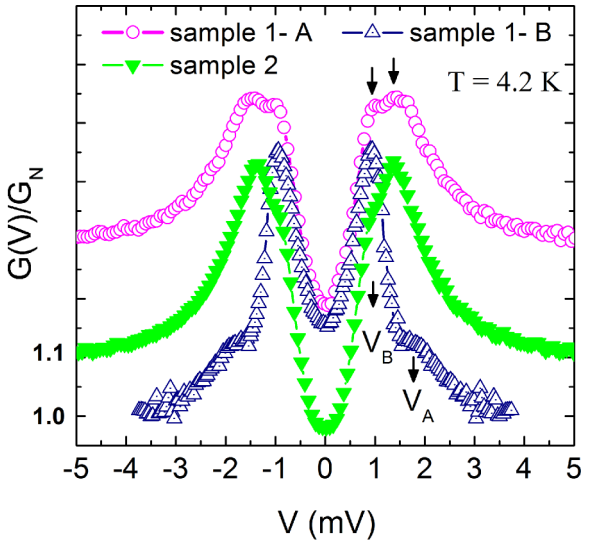

FIG. 4. (Color online) Conductance spectra measured at $T = 4.2$ K for different positions on sample 1 (i.e., A and B) and sample 2 of the $Nb_{0.18}Re_{0.82}$ surface. For clarity, the data are plotted with a constant offset along the linear vertical scale. The symbols are the experimental data and the arrows schematically indicate the positions of the two peaks in the spectrum at voltage biases V_A and V_B.

contact is achieved between the Ag grains and the $Nb_{0.18}Re_{0.82}$ surface. The conductance profile exhibits a rapid drop above the peak at the voltage bias corresponding to the small gap, which gets progressively smoother and broader in energy as the temperature is raised. Moving up in temperature the intensity of the main peak is reduced and the weight between the large and the small gap channels becomes comparable. There is a broadening of the two main peaks with temperature which results in the larger gap having a flat structure with a maximum at about 2.0 meV. The result is that above 6.0 K the high energy shoulder becomes almost featureless. To verify the robustness of the observed features we have repeated the measurements on different regions of the crystal surface as well as on different samples, as shown in Figs. 3(c) and 4. All the measured spectra display a double peak structure as a function of the applied voltage biases with different spectral weight ratios between the two peaks. Furthermore, an inspection of other regions of the sample surface sometimes showed a slight reduction of the energy peak positions which can be attributed to a weak proximity effect in the area of the superconductor that is close to the silver drop. Finally, an analysis of the temperature dependence down to 300 mK confirms the persistence of the double-peak structures observed above 4 K [see Fig. 3(c)].

In order to quantitatively investigate the measured spectra, we adopt the widely used approach based on the Blonder-Thinkham-Klapwijk (BTK) scattering formalism [32] extended to a two-band spectrum. We include the possibility of a quasiparticle lifetime through phenomenological parameters that lead to independent broadening effects in the two bands. We consider a minimal model that is able to capture the features of the conductance spectra. Such a proposal includes isotropic spin-singlet order parameters for each band channel. We assume that the two bands contribute through parallel channels to the charge conductance with a probability p that

is also employed in the fit to tune the weight of each band in the transport. This model has been also applied to successfully describe the conductance spectra of the noncentrosymmetric superconductor BiPd [33].

Hence, the normalized conductance $G(V)/G_N$ can be obtained as a weighted sum of the conductance of two transport channels,

$$\frac{G(V)}{G_N} = p\frac{G_A(V)}{G_{NA}} + (1-p)\frac{G_B(V)}{G_{NB}}, \quad (1)$$

G_N and $G_{NA(B)}$ being the total and the $A(B)$ conductance in the normal state, respectively. Then, $G_A(V)$ and $G_B(V)$ are determined by means of the BTK formalism assuming independent amplitudes for the two isotropic spin-singlet gaps Δ_A and Δ_B, barrier heights Z_A and Z_B, and broadening parameters Γ_A and Γ_B for each channel, respectively. The results are presented in Fig. 3(a) as solid lines and demonstrate a good agreement between the fit and experimental data across the full temperature range. We find that the dominant feature is associated with a smaller gap $\Delta_B = 1.0$ meV and we can resolve a larger gap $\Delta_A = 1.99$ meV at 4.2 K, with a weight $p = 0.12$ for the respective charge conductance channels that has been assumed constant in temperature. The optimal values of the barrier heights are about $Z_A = 8.0$ ($Z_B = 0.5$), thus indicating a regime of low (high) transparency for the large (small) gap channel. The broadening parameters are mainly employed to improve the agreement between the model and the data. The estimated amplitude from the fit turns out to be dependent on the band index and optimal curves can be obtained by assuming a temperature independent Γ with $\Gamma_A = 0.001$ meV and $\Gamma_B = 0$. A scenario emerges where the larger gap is more damped, has a lower probability of carrying electric current, and has a larger effective barrier than the smaller gap. It is worth pointing out that the fitted parameters for a given temperature may be correlated and therefore not unique, especially if one assumes a temperature dependence of the weight p. A similar assumption, for instance, has been used in Ref. [33] for describing the charge conductance of the noncentrosymmetric superconductor BiPd. Here, since a physical justification of such a temperature dependence is not directly linkable to the adopted model, we have performed the fit in a way to optimally reproduce the whole set of data across the full range of temperatures by keeping the amplitude of p unchanged. In Fig. 3(b) we have plotted the temperature dependence of the two gaps as given by the fit to the conductance spectra. One can note that the larger gap has a rapid variation around 5 K which is the temperature above which the second peak gets more suppressed making it difficult to fit the small satellite shoulder at large voltages with high accuracy. The presence of the large gap in the fitting parameters is however necessary for a fairly good match to the charge conductance upon reaching the critical temperature without changing the weight p. On the other hand, the evolution of the small gap is smooth in the full temperature range. Above about 6.5 K the two gaps are almost degenerate in energy. In such a window of temperatures, due to the almost complete suppression of the large voltage peak, there is more uncertainty in the exact determination of the difference between the two gaps.

The double gap features can also be well reproduced within the two-band model for other sets of measurements taken on different positions of the crystal surface. Indeed, the conductance measured at $T = 300$ mK, as reported in Fig. 3(c), can be fairly well described with the two-band model with similar parameters of those used for the fit in Fig. 3(a). The qualitative scenario of two channels with high and low transparency is obtained, i.e., $Z_A = 8.0$ and $Z_B = 0.5$, with a smaller spectral weight $p = 0.12$ associated with the larger gap and the optimal fit yields gap amplitudes of $\Delta_A = 1.55$ meV and $\Delta_B = 1.15$ meV.

Two-peak structures in the conductance with a full gap two-band model do not necessarily imply conventional multiband superconductivity. There are possible alternative scenarios that can qualitatively reproduce the observed conductance spectra. For instance, singlet-triplet mixed-parity superconductors in the presence of Rashba spin-orbit coupling with triplet amplitude Δ_t smaller than the singlet one Δ_s would also produce profiles in the charge conductance with a two-peak structure at energy positions of $\Delta_s - \Delta_t$ and $\Delta_s + \Delta_t$ as discussed more thoroughly in Refs. [34–36]. One of the main drawbacks when trying to apply these models is that a poorer correspondence with the data is found when fitting the relative amplitude of the normalized conductance between the large and the small gap structure. While such a deviation may be cured by a refinement of the model with suitable tuning of the transparency associated with the two spin pairing channels or by adding other microscopic ingredients, the increase of parameters in the fit would make the results less solid and more sensitive to uncontrollable physical variables. In the analyzed case, due to the absence of Andreev midgap states, we note that specific measurements that are able to filter the spin character of the pairing would be required to distinguish between multiband conventional superconductivity and singlet-triplet mixed configurations.

B. Specific heat measurements

In this section we present measurements of the specific heat and its analysis in terms of single- and two-gap models. The specific heat of a single crystal of $Nb_{0.18}Re_{0.82}$, from the same crystal boule as used for the point contact analysis, was measured down to 400 mK in zero field and an applied field of 9 T. The electronic contribution to the specific heat (C_{el}/T) is shown in Fig. 5. This was estimated from fitting the data in the normal state in an applied field of 9 T with $C/T = \gamma + \beta T^2 + \delta T^4$. The outcome is displayed in the inset and $\gamma = 6.1$ mJ/mol K^2, $\beta = 0.039$ mJ/mol K^4, and $\delta = 2.6 \times 10^{-4}$ mJ/mol K^6 are obtained. Hence, the solid line in Fig. 5 shows a fit to the C_{el}/T with a two-band model. The fit consists of a weighted superposition of the specific heat for the single-band case. For a single-band model the superconducting contribution to the entropy is calculated using the following relation:

$$\frac{S}{\gamma T_c} = -\frac{6}{\pi^2}\frac{\Delta_0}{k_B T_c}\int_0^\infty [f\ln f + (1-f)\ln(1-f)]dy, \quad (2)$$

where $f(E)$ is the Fermi-Dirac function with $E = \Delta_0\sqrt{y^2 + \Delta(T)^2}$, y is the energy of the normal state electrons and $\Delta(T)$ is the temperature dependence of the superconducting gap. Both of these quantities have been normalized by $\Delta_0 = \alpha\, k_B T_c$, where the amplitude of α is allowed to vary

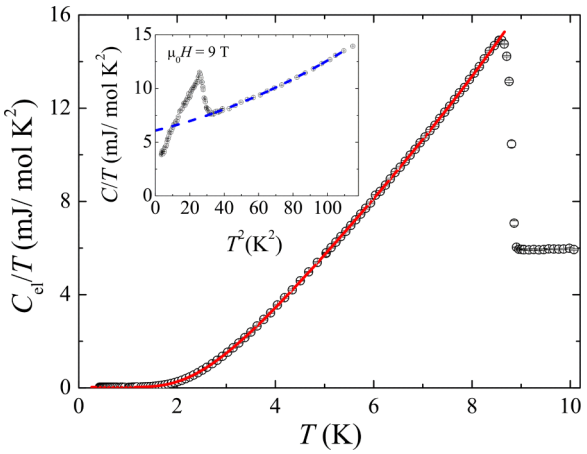

FIG. 5. (Color online) Temperature dependence of the electronic contribution to the specific heat of a single crystal of $Nb_{0.18}Re_{0.82}$ in zero field. The solid line shows a fit to a two-band model, described in the text. The inset shows C/T against T^2, in an applied field of 9 T. The dashed line shows a fit to the data above the transition as described in the text.

from the BCS value of about 1.764. Hence, one can show that the specific heat of the superconducting state can be calculated from the derivative of the entropy with respect to the reduced temperature $t = T/T_c$ using

$$\frac{C_{sc}}{\gamma T} = \frac{d(S/\gamma T_c)}{dt}. \tag{3}$$

Taking into account the expression of the specific heat for the single-band model, an extension to the two-band case can be made by assuming that there are two contributions with different weights

$$\frac{C_{el}}{T} = w\frac{C_{sc}}{T}[\alpha_A] + (1-w)\frac{C_{sc}}{T}[\alpha_B] + c, \tag{4}$$

where $\alpha_{A,B} = \Delta_{A,B}/k_B T_c$, w is the fraction associated with the gap A, and c is a constant. C_{el}/T was fitted by optimizing the parameters in the specific heat and with γ also being allowed to vary in the superconducting state. The results (see Fig. 5) yield magnitudes of $\alpha_A = 2.47$ and $\alpha_B = 1.80$, corresponding to $\Delta_A = 1.86$ meV and $\Delta_B = 1.36$ meV at zero temperature, with $w = 0.32$, indicating that the data are in good agreement with a two-band model.

We point out that the value of γ in the superconducting state is not very correlated with the other parameters and the same value is obtained whether a one- or two-gap fit is made. Thus, this result implies that the slight difference can be an intrinsic aspect of the compound. Furthermore, the conclusions related to the two-gap model are only quantitatively and not qualitatively affected if one does not use γ as a fitting parameter in the superconducting state.

We point out that the fit with a single-band model (not shown here) yields a poorer agreement with the data than the two-band case. However, since it is generally difficult to distinguish between the case of isotropic one- and two-gap models, especially when considering the low temperature range, we have further investigated the full temperature dependence and its derivative in order to extract qualitative elements

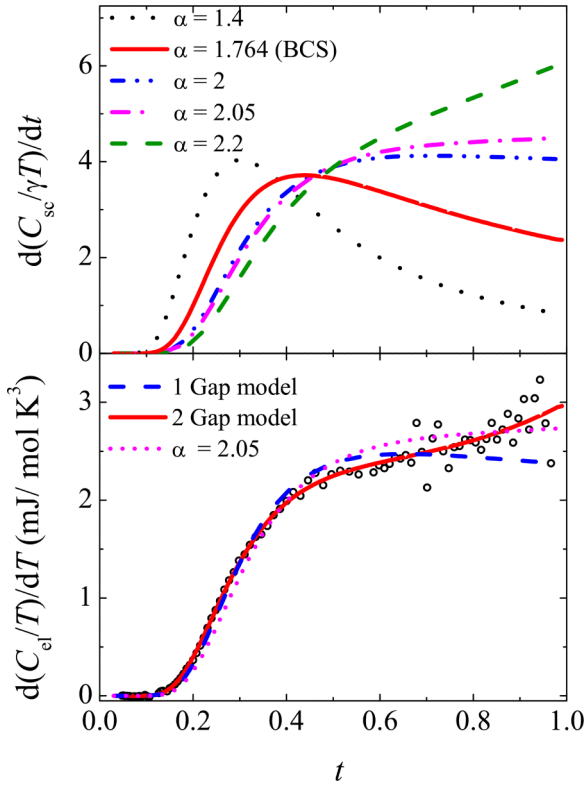

FIG. 6. (Color online) The top panel shows the derivative of the superconducting contribution of the specific heat [Eq. (3)] with respect to the reduced temperature $t = T/T_c$, for several different values of $\alpha = \Delta/k_B T_c$. The bottom panel shows the derivative of the electronic contribution to the specific heat from Fig. 5. The solid line denotes the derivative of the two-band fit in Fig. 5, while the dashed and dotted lines show the derivative of the single band fit with $\alpha = 1.98$ and 2.05, respectively.

to discern between them. Indeed, further evidence for the existence of two energy scales in the specific heat can be found from examining the derivative of C_{sc}/T. This is calculated for several values of α as a function of reduced temperature and is shown in the top panel of Fig. 6. As expected, due to the isotropic structure of the gap, at low temperatures the derivative is flat and its amplitude is close to zero before turning up at higher t and upon increasing α, the temperature at which this upturn occurs also progressively grows. Also, it can be seen that for values of α less than about 2.05, the curves reach a maximum and then decrease towards $t = 1$, while for larger α the curves increase towards the transition. This is a relevant qualitative feature which can be useful to exploit when trying to single out the presence of multiple components in the contribution to the specific heat.

The derivative of the measured C_{el}/T for $Nb_{0.18}Re_{0.82}$ is shown in the bottom panel of Fig. 6. As one can note, the data continues to increase up to $t = 1$ and no maximum is observed at intermediate t, suggesting a gap with $\alpha \geqslant 2.05$. However at low t, the data turns up at too low a temperature for a gap of this magnitude, as shown by the dotted lines. Therefore, such a deviation is evidence for the presence of a smaller energy gap. Fitting the data to an isotropic single band model gives $\alpha = 1.98$. However, as shown by the dashed lines, there is

poor agreement with the data since this predicts a maximum at intermediate t. For completeness we have also reported the derivative of the one-band fit with $\alpha = 2.05$ (dotted line), which clearly indicates how by attempting to reproduce the high-temperature range of data one loses the agreement in the intermediate region of t. On the other hand, as demonstrated by the solid line in Fig. 6, the derivative of the two-gap fit is in good agreement with the data across the full temperature range. It should be noted that in the fit using Eq. (3), there were significant correlations between the parameters w, α_A, and α_B. Therefore, although our results demonstrate that the data are quite compatible with a two-gap model, the values of w, α_A, and α_B may have a small spread and are not unique.

Therefore, we point out that there is a good match between the gap amplitudes extracted from the specific heat measurements and those obtained by point contact spectroscopy. The results show a good agreement for the estimate of both gaps, with a better match for the larger gap value. The discrepancy for the smaller gap amplitude may be attributed to the fact that the point contact probe is more sensitive to the surface and the conductance spectra can be influenced by possible reconstruction or other electronic spectrum modification at the boundary of the superconductor.

IV. CONCLUSIONS

In conclusion, we have analyzed the superconducting state of high-quality single crystals of noncentrosymmetric $Nb_{0.18}Re_{0.82}$ by combining point contact spectroscopy and specific heat measurements. The point contact conductance spectra clearly show a two-peak structure that can be fairly well reproduced within a minimal two-band model. The specific heat measurements provide further evidence for a double-gap structure of the superconducting state. Evidence for two energy scales emerges in the analysis of the temperature dependence of its derivative, where the single-band model clearly fails to reproduce the experimental data. The values of the gaps from the point contact and specific heat measurements are in good agreement, thus providing solid support for a double-gap superconducting state in high-quality single crystals. Though the two-gap isotropic model is sufficient to explain the obtained results, the employed probes are not able to completely single out the spin symmetry of the pairing by excluding the possibility of different scenarios based on mixed spin singlet-triplet pairing. We suggest that further measurements, such as magnetic resonance probes or charge transport analysis in heterostructures having magnetically active elements, which are more sensitive to the spin symmetry of the superconducting pairing, are needed to get deeper insight into the origin of the two gaps.

ACKNOWLEDGMENTS

The work at the University of Warwick was funded by the EPSRC, UK (EP/I007210/1), and by the University of Warwick, through a Research and Development Fund. Some of the equipment used in this research at the University of Warwick was obtained through the Science City Advanced Materials: Creating and Characterising Next Generation Advanced Materials Project, with support from Advantage West Midlands (AWM) and part funded by the European Regional Development Fund (ERDF). This research has received Funding from FP7-REGPOT under Grant No. 264098 – MAMA.

[1] M. Sigrist and K. Ueda, Rev. Mod. Phys. **63**, 239 (1991).
[2] E. Bauer, G. Hilscher, H. Michor, Ch. Paul, E. W. Scheidt, A. Gribanov, Yu. Seropegin, H. Noël, M. Sigrist, and P. Rogl, Phys. Rev. Lett. **92**, 027003 (2004).
[3] E. Bauer and M. Sigrist, *Non-centrosymmetric Superconductors: Introduction and Overview* (Springer, Berlin, 2012), and references therein.
[4] V. M. Edelstein, Zh. Eksp. Teor. Fiz. **95**, 2151 (1989).
[5] L. P. Gor'kov and E. I. Rashba, Phys. Rev. Lett. **87**, 037004 (2001).
[6] P. A. Frigeri, D. F. Agterberg, A. Koga, and M. Sigrist, Phys. Rev. Lett. **92**, 097001 (2004).
[7] I. A. Sergienko and S. H. Curnoe, Phys. Rev. B **70**, 214510 (2004).
[8] A. Harada, S. Akutagawa, Y. Miyamichi, H. Mukuda, Y. Kitaoka, and J. Akimitsu, J. Phys. Soc. Jpn. **76**, 023704 (2007).
[9] S. Kuroiwa, Y. Saura, J. Akimitsu, M. Hiraishi, M. Miyazaki, K. H. Satoh, S. Takeshita, and R. Kadono, Phys. Rev. Lett. **100**, 097002 (2008).
[10] T. Klimczuk, F. Ronning, V. Sidorov, R. J. Cava, and J. D. Thompson, Phys. Rev. Lett. **99**, 257004 (2007).
[11] J. Chen, L. Jiao, J. L. Zhang, Y. Chen, L. Yang, M. Nicklas, F. Steglich, and H. Q. Yuan, New J. Phys. **15**, 053005 (2013).
[12] J. Chen, M. B. Salamon, S. Akutagawa, J. Akimitsu, J. Singleton, J. L. Zhang, L. Jiao, and H. Q. Yuan, Phys. Rev. B **83**, 144529 (2011).
[13] N. Kimura, K. Ito, H. Aoki, S. Uji, and T. Terashima, Phys. Rev. Lett. **98**, 197001 (2007).
[14] R. Settai, Y. Miyauchi, T. Takeuchi, F. Lvy, T. Sheikin, and Y. Onuki, J. Phys. Soc. Jpn. **77**, 073705 (2008).
[15] M. Sato and S. Fujimoto, Phys. Rev. B **79**, 094504 (2009).
[16] Y. Tanaka, T. Yokoyama, A. V. Balatsky, and N. Nagaosa, Phys. Rev. B **79**, 060505(R) (2009).
[17] L. Fang, H. Yang, X. Zhu, G. Mu, Z.-S. Wang, L. Shan, C. Ren, and H.-H. Wen, Phys. Rev. B **79**, 144509 (2009).
[18] N. Kimura, K. Ito, K. Saitoh, Y. Umeda, H. Aoki, and T. Terashima, Phys. Rev. Lett. **95**, 247004 (2005).
[19] N. Tateiwa, Y. Haga, T. D. Matsuda, S. Ikeda, E. Yamamoto, Y. Okuda, Y. Miyauchi, R. Settai, and Y. Onuki, J. Phys. Soc. Jpn. **76**, 083706 (2007).
[20] N. Kimura, Y. Umeda, T. Asai, T. Terashima, and H. Aoki, J. Phys. Soc. Jpn. **76**, 044708 (2007).
[21] P. K. Biswas, A. D. Hillier, M. R. Lees, and D. McK. Paul, Phys. Rev. B **85**, 134505 (2012).
[22] R. P. Singh, A. D. Hillier, B. Mazidian, J. Quintanilla, J. F. Annett, D. McK. Paul, G. Balakrishnan, and M. R. Lees, Phys. Rev. Lett. **112**, 107002 (2014).
[23] A. B. Karki, Y. M. Xiong, N. Haldolaarachchige, S. Stadler, I. Vekhter, P. W. Adams, D. P. Young, W. A. Phelan, and J. Y. Chan, Phys. Rev. B **83**, 144525 (2011).
[24] C. S. Lue, T. H. Su, H. F. Liu, and B.-L. Young, Phys. Rev. B **84**, 052509 (2011).

[25] J. Chen, L. Jiao, J. L. Zhang, Y. Chen, L. Yang, M. Nicklas, F. Steglich, and H. Q. Yuan, Phys. Rev. B **88**, 144510 (2013).
[26] R. P. Singh, M. Smidman, M. R. Lees, D. McK. Paul, and G. Balakrishnan, J. Cryst. Growth **361**, 129 (2012).
[27] D. Daghero and R. S. Gonnelli, Supercond. Sci. Technol. **23**, 043001 (2010).
[28] R. S. Gonnelli, D. Daghero, G. A. Ummarino, V. A. Stepanov, J. Jun, S. M. Kazakov, and J. Karpinski, Phys. Rev. Lett. **89**, 247004 (2002).
[29] S. Sasaki, M. Kriener, K. Segawa, K. Yada, Y. Tanaka, M. Sato, and Y. Ando, Phys. Rev. Lett. **107**, 217001 (2011).
[30] S. Sasaki, Z. Ren, A. A. Taskin, K. Segawa, L. Fu, and Y. Ando, Phys. Rev. Lett. **109**, 217004 (2012).
[31] D. Daghero, A. Calzolari, G. A. Ummarino, M. Tortello, R. S. Gonnelli, V. A. Stepanov, C. Tarantini, P. Manfrinetti, and E. Lehmann, Phys. Rev. B **74**, 174519 (2006).
[32] G. E. Blonder, M. Tinkham, and T. M. Klapwijk, Phys. Rev. B **25**, 4515 (1982).
[33] M. Mondal, B. Joshi, S. Kumar, A. Kamlapure, S. C. Ganguli, A. Thamizhavel, S. S. Mandal, S. Ramakrishnan, and P. Raychaudhuri, Phys. Rev. B **86**, 094520 (2012).
[34] C. Iniotakis, N. Hayashi, Y. Sawa, T. Yokoyama, U. May, Y. Tanaka, and M. Sigrist, Phys. Rev. B **76**, 012501 (2007).
[35] J. Linder and A. Sudbø, Phys. Rev. B **76**, 054511 (2007).
[36] P. Burset, F. Keidel, Y. Tanaka, N. Nagaosa, and B. Trauzettel, Phys. Rev. B **90**, 085438 (2014).